Optics Letters

Low-spatial-coherence high-radiance broadband fiber source for speckle free imaging

Brandon Redding,[1] Peyman Ahmadi,[2] Vadim Mokan,[2] Martin Seifert,[2] Michael A. Choma,[1,3,4] and Hui Cao[1,*]

[1]Department of Applied Physics, Yale University, New Haven, Connecticut 06520, USA
[2]Nufern, East Granby, Connecticut 06026, USA
[3]Departments of Diagnostic Radiology and Pediatrics, Yale School of Medicine, New Haven, Connecticut 06520, USA
[4]Department of Biomedical Engineering, Yale University, New Haven, Connecticut 06520, USA
*Corresponding author: hui.cao@yale.edu

Received 5 June 2015; revised 17 August 2015; accepted 3 September 2015; posted 8 September 2015 (Doc. ID 242218); published 6 October 2015

We design and demonstrate a fiber-based amplified spontaneous emission (ASE) source with low spatial coherence, low temporal coherence, and high power per mode. ASE is produced by optically pumping a large gain core multimode fiber while minimizing optical feedback to avoid lasing. The fiber ASE source provides 270 mW of continuous wave emission, centered at $\lambda = 1055$ nm, with a full width at half-maximum bandwidth of 74 nm. The emission is distributed among as many as ~70 spatial modes, enabling efficient speckle suppression when combined with spectral compounding. Finally, we demonstrate speckle-free full-field imaging using the fiber ASE source. The fiber ASE source provides a unique combination of high power per mode with both low spatial and low temporal coherence, making it an ideal source for full-field imaging and ranging applications.

OCIS codes: (140.3510) Lasers, fiber; (060.2320) Fiber optics amplifiers and oscillators; (030.6140) Speckle.

http://dx.doi.org/10.1364/OL.40.004607

Traditional amplified spontaneous emission (ASE) light sources combine broadband emission, similar to a light emitting diode (LED), with high spatial coherence and high power per mode, similar to a laser. This combination, realized in both fiber-based ASE sources [1] and semiconductor-based superluminescent diodes (SLD) [2], has made ASE sources increasingly popular for a range of applications including spectroscopy [3], optical coherence tomography (OCT) [4], fiber sensors [5], and gyroscopes [6]. However, the high spatial coherence of existing ASE sources has precluded their use in full-field imaging applications, where spatial coherence introduces artifacts such as speckle. By comparison, traditional low spatial coherence sources such as thermal sources and LEDs do not provide the required power per mode for high-speed, full-field imaging applications [7]. Recently, there have been several demonstrations of multimode lasers that combine low spatial coherence with high power per mode, including dye-based random lasers [8,9], powder-based random Raman lasers [10], solid-state degenerate lasers [11,12], semiconductor-based chaotic microcavity lasers [13], and semiconductor-based large-area vertical cavity surface emitting lasers (VCSELs) [14–16] and VCSEL arrays [17]. However, an optical-fiber based light source with low spatial coherence has not been demonstrated. In addition, each of these previous demonstrations of low spatial coherence lasers provided narrow bandwidth emission with relatively high temporal coherence, precluding their use in ranging applications such as OCT [18] or frequency resolved lidar [19].

In this Letter, we present a novel fiber-based ASE source that combines low temporal and low spatial coherence, similar to an LED, with the high power per spatial mode associated with lasers and traditional single spatial-mode ASE sources. The fiber ASE source provides 270 mW of continuous wave (CW) emission centered at $\lambda = 1055$ nm with 74 nm 3 dB bandwidth (full width at half-maximum). The emission is distributed among as many as 70 spatial modes, enabling efficient speckle suppression when combined with spectral compounding. We also demonstrate speckle-free full-field imaging using the fiber ASE source. By providing broadband, speckle-free emission with ~40 dB higher power per mode than an LED, the fiber ASE source is ideally suited for high-speed, full-field imaging and coherent ranging applications.

To achieve highly multimode emission from an optical fiber, we used a recently developed optical fiber with an extra-large mode area (XLMA) gain core [20]. The basis of the XLMA design is synthetic fused bulk silica doped with ytterbium (Yb) and other codopants that form the active core of the fiber. This rare-earth-doped bulk silica is commercialized by Heraeus Quarzglas (Kleinostheim, Germany). The XLMA fiber used in our ASE source has a 100 μm diameter, a Yb-doped core with numerical aperture (NA) of 0.1 that is surrounded by a 400 μm diameter octagonal inner cladding, and a 480 μm diameter outer cladding (Nufern XLMA-YTF-95/400/480). A Yb concentration of 1000 ppm in the core results in 7.8 dB/m absorption at 972 nm. The inner cladding provides guiding for the pump light, thus it

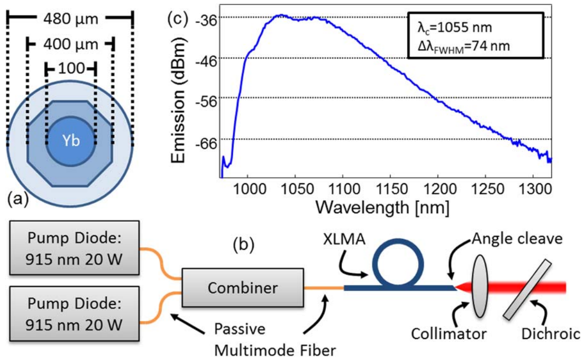

Fig. 1. (a) Cross section of the Yb-doped XLMA fiber. (b) Schematic of the ASE source. (c) The emission spectrum from the fiber ASE source.

is also called the pump core in contrast to the gain core that guides the emitted light. A schematic of the XLMA fiber cross section is shown in Fig. 1(a). We estimated the number of transverse spatial modes supported in the Yb-doped gain core of the fiber to be $M = 16R^2(\mathrm{NA})^2/\lambda^2 = 360$ at $\lambda = 1050$ nm, where R is the core radius [21]. The XLMA fiber was optically pumped using two 20 W laser diodes operating at $\lambda = 915$ nm. A fiber combiner was used to couple the output beams from the two pump diodes into the pump core of a 4.4 meter long piece of XLMA fiber, as shown schematically in Fig. 1(b). The end of the fiber was cleaved at an angle of 4° to minimize feedback, which could lead to lasing. Minimization of feedback ensured that the fiber operated as a broadband ASE source with low temporal coherence [22]. Emission from the end of the XLMA was then collimated, and the remaining 915 nm pump light was filtered out by a dichroic filter.

We then characterized the emission of the fiber ASE source using a power meter and an optical spectrum analyzer. The fiber ASE source produced 270 mW of CW emission with a center wavelength of 1055 nm and a 3 dB bandwidth of 74 nm, as shown in Fig. 1(c). The emission power exhibited a superlinear increase with pump power above a threshold of ~22 W. We did not observe saturation in the output power at the maximum pump power of 40 W, indicating that higher emission should be possible by incorporating additional pump diodes. The relatively low quantum efficiency of the current fiber ASE source is due to a mode mismatch between the passive multimode fiber of the combiner and the octagonal pump core of the XLMA fiber, which significantly reduced the amount of pump light coupled into the XLMA fiber. In addition, approximately half of the fiber ASE was in the counter-propagating direction of the pump light and not collected in our experiments. Nonetheless, the 270 mW emission in the co-propagating direction is sufficient for many imaging applications and allowed us to characterize the spatial and temporal coherence of the XLMA fiber ASE source. Moreover, the fiber ASE source already provides ~4 mW/nm, which is comparable to commercially available supercontinuum sources [23].

We then characterized the ability of the fiber ASE source to suppress speckle formation. Speckle is a coherent artifact known to corrupt image formation and can be characterized by the speckle contrast $C = \sigma_I/\langle I\rangle$, where σ_I is the standard deviation of the intensity and $\langle I\rangle$ is the average intensity [24]. A recent study on the human perception of speckle found that speckle with contrast below ~0.04 could not be detected, providing a guideline for the development of a light source with sufficiently low spatial coherence for imaging [25].

To measure the speckle pattern formed by a light source, we collimated the emission, forming a 2 mm diameter beam onto a ground-glass diffuser and recorded images of the transmitted light within ±8° on a CCD camera (Allied Vision Mako-G125B) positioned ~3 cm behind the diffuser. For comparison, we first measured the speckle pattern formed by light from one of the 915 nm pump diodes. As shown in Fig. 2(a), the spatially coherent 915 nm pump diode produced a clear speckle pattern with contrast of ~0.46. The speckle contrast was less than unity since the pump diode consists of a few separate emitters coupled into a multimode fiber. We then repeated the experiment while illuminating the diffuser with emission from the fiber ASE source, which produced the image shown in Fig. 2(b). The uniform intensity across the image confirmed that the fiber ASE source efficiently suppressed speckle formation. Based on the image in Fig. 2(b), we calculated a speckle contrast of ~0.02, below the threshold required to avoid human detection in an imaging setting.

In addition to the 100 µm diameter XLMA fiber, we tested speckle formation using two additional ASE sources: a fiber ASE source based on a 30 µm diameter, 5 meter long, Yb-doped fiber (Nufern LMA-YDF-30/400-VIII, NA = 0.06; East Granby, Connecticut, USA) that supports ~10 spatial modes at $\lambda = 1050$ nm [21] and a commercially available, semiconductor-based multimode superluminescent diode (Superlum M-381). The 30 µm diameter fiber ASE source produced moderately broadband emission with a 3 dB bandwidth of ~20 nm; however, as shown in Fig. 2(c), the emission also produced speckle with contrast of ~0.42. The multimode SLD provided ~150 mW of power at $\lambda = 800$ nm with a 3 dB bandwidth of 40 nm. Nonetheless, emission from the SLD still produced speckle with contrast of ~0.2. Thus, the XLMA fiber ASE source was the only ASE source that has been realized so far that suppressed speckle to acceptable levels for full-field imaging applications.

The speckle contrast depends on the number of mutually incoherent spatial modes present in the illumination. Different spatial modes produce distinct speckle patterns, which sum in intensity, thereby reducing the speckle contrast to $C = M^{-1/2}$, where M is the number of spatial modes [24]. Of course, even if the XLMA fiber ASE was distributed equally among all ~360 passive modes of the fiber, we would naively expect the speckle contrast to be reduced to only $360^{-1/2} = 0.05$. However, the

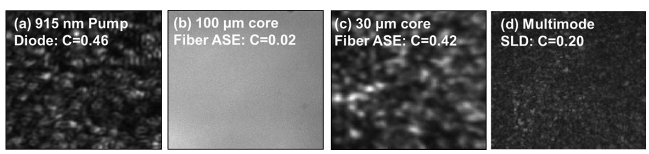

Fig. 2. Speckle formed by light incident on a camera after passing through a diffuser. (a) The pump diode used to pump the fiber ASE source produced speckle with contrast of 0.46. (b) The 100 µm diameter gain core, XLMA fiber ASE efficiently suppressed speckle, with a measured contrast of 0.02. (c) ASE from a fiber with a 30 µm diameter gain core produced speckle with contrast of 0.42. (d) ASE from a multimode SLD produced speckle with contrast of 0.2.

measured speckle shown in Fig. 2(b) had a lower contrast of 0.02, indicating that additional effects were present. The ASE was unpolarized; thus the two independent polarization states reduced the speckle contrast by a factor of $2^{-1/2} = 1.4$. Moreover, the broadband ASE enabled spectral compounding, as different spectral modes can also contribute to the speckle reduction. Still, it remains difficult to estimate just how many spatial modes are excited from the spectrally integrated speckle patterns measured above. Also the number of spatial modes at any given wavelength is important for applications such as spectral-domain OCT, in which a spectrally resolved detection would limit the effect of spectral compounding.

To separate the effect of averaging over the spatial modes from the effect of spectral compounding, we then measured the speckle pattern at individual wavelengths using an imaging spectrometer (Acton Research SpectraPro 300i). To do this, we coupled the emission from the fiber ASE source to a passive, 1 meter long multimode fiber (105 μm-diameter core, NA = 0.22). The distal end of the multimode fiber was then collimated onto the entrance slit of an imaging spectrometer. At the exit port of the spectrometer, a CCD camera (Andor Newton) recorded the spectrally dispersed 1D speckle. In the 2D image taken by the CCD camera, the horizontal axis corresponded to wavelength, and the vertical axis corresponded to space. In this measurement, the multimode fiber played the role of the diffuser, producing distinct speckle patterns for different spatial modes of the ASE source, while efficiently coupling light into the entrance slit of the spectrometer. However, the speckle patterns formed at the end of a multimode fiber are known to vary as a function of wavelength [26], and a sufficiently long multimode fiber, combined with a broadband light source, can effectively reduce the spatial coherence [27,28]. To confirm that the multimode fiber did not reduce the measured speckle contrast for individual spectral channels resolved by the spectrometer, we first coupled a spatially coherent supercontinuum source (Fianium WhiteLase SC400-4) into the multimode fiber. As shown in Fig. 3(a), the supercontinuum source produced high-contrast speckle in space at each wavelength. The spectral correlation of the speckle pattern (corresponding to the spectral correlation of the multimode fiber) was readily resolved by the spectrometer, indicating that the spectral correlation width of the fiber (∼0.8 nm) is larger than the spectral resolution of the spectrometer (∼0.2 nm). Moreover, the contrast of the speckle produced by the supercontinuum emission coupled through the multimode fiber was ∼0.5, corresponding to the average of four speckle patterns. These four speckle patterns were produced by the two polarization states of the supercontinuum emission (which is unpolarized), each of which was then scrambled by the passive multimode fiber to produce two distinct speckle patterns with orthogonal polarization. This confirms that the multimode fiber will not reduce the contrast of the spectrally resolved speckle pattern produced by the fiber ASE source.

We then repeated the experiment using the fiber ASE source. The spectrally dispersed speckle pattern formed by the fiber ASE source is shown in Fig. 3(b). The speckle contrast at any given wavelength is clearly reduced in comparison to the supercontinuum source due to the presence of many spatial modes in the fiber ASE. Based on the image in Fig. 3(b), we then calculated the spectrally resolved speckle contrast, as shown in Fig. 3(c). From this contrast, we then estimated

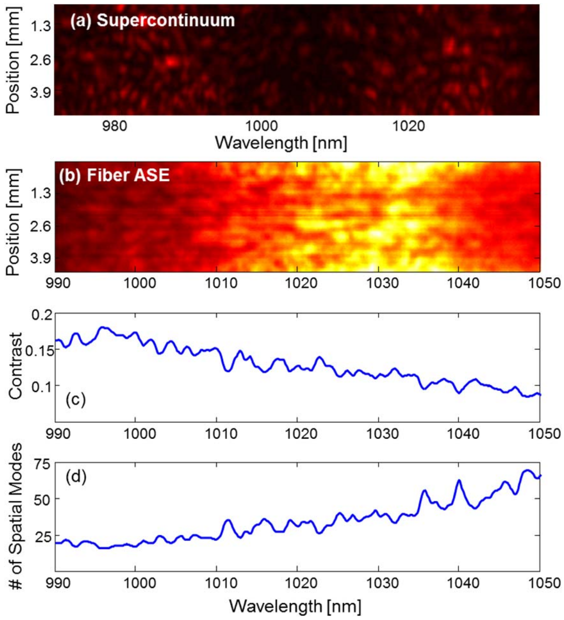

Fig. 3. (a) Spectrally dispersed speckle pattern formed by coupling emission from a supercontinuum source through a multimode fiber into an imaging spectrometer. The spectrometer is able to resolve the spectrally varying speckle, confirming that the fiber does not reduce the measured speckle contrast at a given wavelength. (b) Spectrally dispersed speckle pattern formed by the fiber ASE. (c) Spectrally resolved speckle contrast calculated from the 1D speckle pattern at each wavelength in (b). (d) The number of spatial modes present at each wavelength calculated from the spectrally resolved speckle contrast.

the number of spatial modes present at each wavelength, $M = C^{-2}/2$, where the factor of 2 accounts for polarization mixing in the multimode fiber. Figure 3(d) shows that the number of spatial modes increased with wavelength from ∼25 at $\lambda = 990$ nm to almost 75 spatial modes at $\lambda = 1050$ nm, near the peak of the emission spectrum. This also explains the low speckle contrast shown in Fig. 2(b). Because the spectral correlation width of the ground-glass diffuser was ∼6.7 nm in our experiment, the emission was distributed in ∼11 spectral channels, each of which had, on average, ∼50 spatial modes and two polarization states. In total, ∼1, 100 uncorrelated speckle patterns were generated, giving a speckle contrast of ∼0.03, which is close to the experimentally measured contrast of 0.02. Note that, due to the responsivity of the Si CCD camera used to record the spectrally dispersed speckle patterns, we were unable to measure the number of modes present in the long-wavelength half of the emission spectrum. Nonetheless, Fig. 3(d) illustrates that the number of spatial modes increases from the tail to the center of the gain spectrum. We also note that although the XLMA fiber supports ∼360 passive modes, the emission was distributed among less than one-fourth of these modes, even at the peak of the gain spectrum. This could be the result of increased bending loss experienced by the higher order modes and/or the mode competition for gain. Nonetheless, the XLMA fiber ASE source distributed emission among many more spatial modes than the multimode SLD, enabling efficient speckle suppression where the SLD did not.

In addition to the low spatial coherence, the temporal coherence of the fiber ASE source is also low, which is well suited for

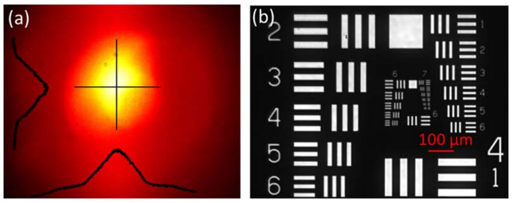

Fig. 4. (a) Spatial profile of the output beam from the fiber ASE source. (b) An image of a US Air Force resolution chart illuminated in transmission by the fiber ASE source.

ranging applications such as OCT or frequency-resolved coherent lidar [19]. For example, the 3 dB bandwidth of 74 nm would provide an axial resolution of 6.6 μm in OCT (assuming a refractive index of 1). In addition to providing both low spatial and low temporal coherence, the fiber ASE source also exhibits high directionality, with a divergence angle of less than 6° (dictated by the NA = 0.1 of the fiber). Despite the participation of many spatial modes, the spatial profile of the output beam from the fiber ASE source is smooth and well suited for illumination in imaging applications, as confirmed by the image of the collimated beam in Fig. 4(a). Finally, we used the fiber ASE as an illumination source to image a US Air Force resolution chart through a static ground glass in transmission mode. A speckle-free full-field image was obtained as shown in Fig. 4(b).

While the fiber ASE source provides speckle-free illumination similar to a thermal source or LED, it also produces much higher power per mode, which could enable high-speed imaging or illumination at large distances. As a quantitative comparison, we calculated the photon degeneracy, which describes the number of photons per coherence volume. The photon degeneracy parameter is represented by $\delta = (P\delta z)/(h\nu cM)$, where P is the emission power, δz is the temporal coherence length, $h\nu$ is the photon energy, c is the speed of light, and M is the number of spatial modes [29]. Based on our measurement shown in Fig. 3, revealing that the fiber ASE is distributed on average among ~50 spatial modes, we calculated a photon degeneracy of $\delta \sim 600$. This is more than four orders of magnitude higher than the photon degeneracy of a thermal source (e.g., at 4000 K temperature and $\lambda = 1050$ nm, $\delta \sim 10^{-2}$ [29]) and a bright LED ($\delta \sim 10^{-2}$). It is also competitive with a recent demonstration of a relatively narrowband, low-spatial-coherence chaotic microcavity laser ($\delta \sim 100$) [13]. In addition, the high-power commercial SLD shown to produce speckle of contrast ~0.2 in Fig. 2(d) exhibits similar degeneracy of $\delta \sim 600$, despite maintaining relatively high spatial coherence and a low number of spatial modes.

In summary, we have demonstrated a fiber ASE source that combines high power per mode with low spatial and low temporal coherence. The ASE source provides 270 mW of CW emission with 74 nm 3 dB bandwidth centered at $\lambda = 1055$ nm. We characterized the spatial coherence and found that the emission is distributed among as many as ~70 spatial modes. A further increase of the number of spatial modes is possible by increasing gain or using a fiber with a larger gain core. The emission exhibits a small divergence angle and uniform spatial profile, making it well suited as an illumination source in full-field imaging and ranging applications. In the future, we expect the pump efficiency and output power of the fiber ASE source will be dramatically improved by matching the geometry of the passive multimode fiber to the pump core of the XLMA fiber.

Funding. National Institutes of Health (NIH) (1R21EB016163-01A1, 1R21HL125125-01A1); Office of Naval Research (ONR) (MURI SP0001135605).

Acknowledgment. We thank Yaron Bromberg for useful discussions and thank Seng Fatt Liew and Wen Xiong for experimental assistance.

REFERENCES

1. P. Wang, J. K. Sahu, and W. A. Clarkson, Opt. Lett. **31**, 3116 (2006).
2. M. Rossetti, J. Napierala, N. Matuschek, U. Achatz, M. Duelk, C. Vélez, A. Castiglia, N. Grandjean, J. Dorsaz, and E. Feltin, Proc. SPIE **8252**, 825208 (2012).
3. W. Denzer, M. L. Hamilton, G. Hancock, M. Islam, C. E. Langley, R. Peverall, and G. A. D. Ritchie, Analyst **134**, 2220 (2009).
4. A. F. Fercher, W. Drexler, C. K. Hitzenberger, and T. Lasser, Rep. Prog. Phys. **66**, 239 (2003).
5. H. S. Choi, H. F. Taylor, and C. E. Lee, Opt. Lett. **22**, 1814 (1997).
6. B. Lee, Opt. Fiber Technol. **9**, 57 (2003).
7. B. Karamata, M. Leutenegger, M. Laubscher, S. Bourquin, T. Lasser, and P. Lambelet, J. Opt. Soc. Am. A **22**, 1380 (2005).
8. B. Redding, M. A. Choma, and H. Cao, Nat. Photonics **6**, 355 (2012).
9. A. Mermillod-Blondin, H. Mentzel, and A. Rosenfeld, Opt. Lett. **38**, 4112 (2013).
10. B. H. Hokr, M. S. Schmidt, J. N. Bixler, P. N. Dyer, G. D. Noojin, B. Redding, R. J. Thomas, B. A. Rockwell, H. Cao, V. V. Yakovlev, and M. O. Scully, "A narrow-band specklefree light source via random Raman lasing," (in review) arXiv: 1505.07156 (2015).
11. M. Nixon, B. Redding, A. A. Friesem, H. Cao, and N. Davidson, Opt. Lett. **38**, 3858 (2013).
12. R. Chriki, M. Nixon, V. Pal, C. Tradonsky, G. Barach, A. A. Friesem, and N. Davidson, Opt. Express **23**, 12989 (2015).
13. B. Redding, A. Cerjan, X. Huang, M. Larry, A. D. Stone, and M. A. Choma, Proc. Natl. Acad. Sci. USA **112**, 1304 (2015).
14. F. Riechert, G. Verschaffelt, M. Peeters, G. Bastian, U. Lemmer, and I. Fischer, Opt. Commun. **281**, 4424 (2008).
15. G. Craggs, G. Verschaffelt, S. K. Mandre, H. Thienpont, and I. Fischer, IEEE J. Sel. Top. Quantum Electron. **15**, 555 (2009).
16. G. Verschaffelt, G. Craggs, M. L. F. Peeters, S. K. Mandre, H. Thienpont, and I. Fischer, IEEE J. Quantum Electron. **45**, 249 (2009).
17. J.-F. Seurin, G. Xu, V. Khalfin, A. Miglo, J. D. Wynn, P. Pradhan, C. L. Ghosh, and L. A. D'Asaro, Proc. SPIE **7229**, 722903 (2009).
18. W. Drexler and J. G. Fujimoto, *Optical Coherence Tomography* (Springer-Verlag, 2008).
19. W. C. Swann and N. R. Newbury, Opt. Lett. **31**, 826 (2006).
20. A. Langner, G. Schötz, M. Such, T. Kayser, V. Reichel, S. Grimm, J. Kirchhof, V. Krause, and G. Rehmann, Proc. SPIE **6873**, 687311 (2008).
21. K. Okamoto, *Fundamentals of Optical Waveguides* (Elsevier, 2006).
22. D. Marcuse, Appl. Opt. **14**, 3016 (1975).
23. N. Savage, Nat. Photonics **3**, 114 (2009).
24. J. W. Goodman, *Speckle Phenomena in Optics* (Roberts & Company, 2007).
25. S. Roelandt, Y. Meuret, A. Jacobs, K. Willaert, P. Janssens, H. Thienpont, and G. Verschaffelt, Opt. Express **22**, 23965 (2014).
26. B. Crosignani, B. Daino, and P. Di Porto, J. Opt. Soc. Am. **66**, 1312 (1976).
27. N. Takai and T. Asakura, J. Opt. Soc. Am. A **2**, 1282 (1985).
28. J. Kim, D. T. Miller, E. Kim, S. Oh, J. Oh, and T. E. Milner, J. Biomed. Opt. **10**, 064034 (2005).
29. L. Mandel and E. Wolf, *Optical Coherence and Quantum Optics* (Cambridge University, 1995).